

The decay of grid turbulence in polymer and surfactant solutions

Eric van Doorn, Christopher M. White, and K. R. Sreenivasan
Mason Laboratory, Yale University, New Haven, Connecticut 06520-8286

(Received 23 September 1998; accepted 3 May 1999)

The decay of turbulence behind a towed grid is studied in polymer and surfactant solutions with the use of particle image velocimetry. Unlike in water, the turbulent energy components show marked anisotropy, and decay more slowly. These differences are stronger for initial periods of time, but persist through the entire period of decay. The major difference between the polymer and surfactant solutions is that the small scales are more strongly damped in the former. © 1999 American Institute of Physics. [S1070-6631(99)04108-2]

I. INTRODUCTION

It is known for about 50 years that small amounts of long-chain polymers or surfactants, when added to turbulent water flows, have an incommensurately large macroscopic effects, for instance, a few tens of parts per million (by weight) of a polymer can reduce the pressure drop in a pipe flow by as much as 80%. Many research articles¹ have appeared on the interaction between turbulence and drag reducing agents (DRAs), and those by Lumley,² Virk,³ de Gennes,⁴ and Den-Toonder *et al.*⁵ may be said to represent some prevailing perspectives on the problem. Despite the immense volume of work,¹ the physics of the interaction of turbulence with DRAs is not adequately understood. One of the unresolved questions concerns the distinctly different ways in which the polymer works in the wall-region and in the outer region of a wall-bounded flow. The effort expended on answering this particular question is also large, but the outcome again is not definitive;⁶ part of the difficulty is that one does not fully understand the role of the wall and outer regions in creating and maintaining turbulence in ordinary pipe or boundary layer flows.⁷ It therefore seemed helpful to understand the effects of the polymer in homogeneous turbulent flows where wall effects play no direct role. This is our first goal.

This same goal has prompted previous measurements in turbulence behind grids.^{8,9} However, the conclusions there were somewhat obscured by the unreliability of hot-film probes in polymer solutions. We have bypassed this problem by using particle image velocimetry (PIV). To our knowledge, there has been only one other noninvasive study of polymer solutions in grid turbulence.⁹ This study, using laser Doppler anemometry, showed that polymer additives in grid turbulence lower the rate of decay and suppress small scale components above a threshold concentration. These results seem to support the notion that polymers affect turbulence outside of the wall region, but are limited in two respects. First, the benchmark results for water were not fully satisfactory. Second, since the measurements were pointwise and only one component of turbulence was obtained, neither the anisotropy (even in grid turbulence, as we shall see presently) nor the spatial structure could be studied. The PIV technique acquires two-component velocity data in a two-

dimensional slice of the flow field, and so provides some information regarding the anisotropy and the flow structure.

The papers by Friehe and Schwartz⁸ and McComb *et al.*⁹ concerned polymers. Recently, there has been an increasing interest in surfactant DRAs.^{10,11} The experimental evidence in these and other papers suggests that the mechanism for drag reduction for surfactants may be different from that for polymer solutions, but the number and quality of papers on surfactant effects lag behind those for polymers. In particular, experiments comparing surfactants and polymers in the same apparatus are rare; indeed, we know of only one such experiment¹¹ in pipe flow. It thus seemed valuable to compare polymers and surfactants in the simpler case of turbulence behind a towed grid. We believe that our data are the first of their kind, this being the second reason for the paper.

In the next section, we present experimental details of the work, while Sec. III describes the principal results. Interpretations and discussions are summarized in Sec. IV.

II. EXPERIMENT

We performed experiments in a $30 \times 30 \times 120$ cm³ plate-glass tank, filled with the fluid. The grid had a square mesh of size $M = 1.27$ cm and solidity $\sigma = 0.44$. This solidity is comparable to those in most standard experiments on grid turbulence (see Sreenivasan¹² for a summary). For purposes of comparison, we first studied the decay of turbulence behind the towed grid in ordinary tap water. This was followed up by similar studies in three dilute solutions of Polyethylene Oxide (Polyox grade COAG) and two surfactant solutions (Ethoquad T/13/50 produced by Akzo Nobel). All three polymer concentrations were typical of those used in drag reduction studies. For these concentrations, the shear viscosity of the solution exceeded that of water by only small amounts; for the highest polymer concentration, the solution viscosity was 18% more than that of water (see Table I). Within this limit, the increase in shear viscosity was linear with polymer concentration. The solutions were thus considered dilute. The surfactant was of the cationic type (tallow tris-hydroxyethyl ammonium acetate). We used two different surfactant concentrations, both comparable to those used in drag reduction studies in pipe flows. In contrast to polymers, the surfactant concentrations were large enough to increase

TABLE I. Table of viscosities for water as well as polymer and surfactant solutions of various concentrations. For surfactants, the concentration is denoted by two numbers. The first denotes the concentration of the surfactant itself, the second the concentration of sodium salicylate.

Fluid (concentration)	Viscosity (cp)
polymer (100 ppm)	1.18
polymer (50 ppm)	1.08
polymer (25 ppm)	1.05
surfactant (5.0 mM/12.0 mM)	6.1
surfactant (2.2 mM/4.8 mM)	2.8
water	1.0

the shear viscosity significantly, by as much as six times that of water at the highest concentration. Since it is known that cationic surfactant solutions are drag-reducing only in the presence of an appropriate counterion salt, we doped them with sodium salicylate (Table I). This is believed to promote the formation of rodlike micelles—apparently a necessary condition for drag reduction.¹⁰

For all cases, the grid was towed at the speed $U = 2.5$ m/s from the bottom to the top of tank. For water, the Reynolds number based on mesh size $R_M \approx 32000$. The direction of motion of the grid was taken to be the *longitudinal* direction, x . Perpendicular to the longitudinal direction (but in the plane of the camera) was the *transverse* direction, y (Fig. 1).

The flow in a vertical slice A in the central region of the tank was mapped by means of a two-color particle image velocimetry (PIV) system (Fig. 1). The dimensions of the slice were $2.17 \times 1.44 \times 0.1$ cm. A digital color-camera captured the scattered light from nearly neutrally buoyant seeding particles. The seeding was done with polydisperse aluminum oxide particles with typical diameter of the order ≤ 10 μm . A simple estimate¹³ of the velocity lag due to the density difference between water and aluminum oxide is 5 $\mu\text{m/s}$ or about 0.5% for a typical velocity of 1 mm/s. After adding the seeding particles to the tank and mixing its contents, several hours of wait preceded the experiment. This waiting time allowed the largest seeding particles to settle to the tank bottom. We added sufficient amount of seeding material to ensure an adequate particle image density (about 10 per interrogation volume) for a successful PIV interrogation, and determined this seeding density *a posteriori* to be $\approx 10^{-5}$ by mass fraction.

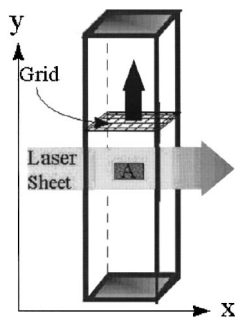


FIG. 1. The schematic of the tank. The imaged area A is not to scale.

The laser illumination consisted of a red light sheet and a green light sheet, superimposed in space but separated in time by a few milliseconds. We used two different colors to resolve the directional ambiguity that limits more traditional PIV schemes. The green light (532 nm) was generated with a pulsed Nd-YAG laser with a pulse length of 6 ms and 135 mJ peak energy. The red (607 nm) light was generated by passing the light of an identical laser through a Raman cell. The Raman cell was filled with a 50–50 mixture of N_2 and He gases at 1050 psi; this generated the red light with an efficiency of about 30%. The two beams were superimposed by means of a dichromic mirror. The light sheets were formed with two spherical lenses, and one cylindrical lens.¹³ Over the extent of the imaged area, the light sheet thickness did not exceed 1 mm.

A set of PIV images was taken at a fixed delay ΔT after the grid passed the imaged area. The time of acquisition of the PIV images varied between $50t_M < \Delta T < 2 \times 10^4 t_M$, where t_M , the characteristic time scale, is given by M/U . Large decay times of the order of $10^4 t_M$ can be probed only in towed grid experiments; in wind tunnels with the flow past a grid, the usual range covered is only a few hundred mesh distances.

For each value of ΔT , we used an ensemble of 36 images for water, of 24 images for polymer solutions, and mostly 15 images, occasionally 12, for surfactant solutions. (The reasons for the smaller size of surfactant data will become clear momentarily.) Pulling the grid through the polymer and surfactant solutions did not affect subsequent sequences of measurements, thereby ruling out polymer (and surfactant) degradation.

After the experiment, the images were transferred from the digital color camera to a PC. A cross-correlation PIV analysis between the red and the green field of each image yielded the two-dimensional projection of the flow field in A on the x - y plane. The camera's CCD array was 1524×1012 pixels. The magnification was such that 1 pixel corresponded to 14.2 μm . For averaging purposes, we used cells of 64×64 pixels, with adjoining cells 16 pixels apart.

Since an important step in polymer and surfactant experiments was the proper preparation of the solutions, the procedure calls for some comments. We prepared the polymer solution by suspending the Polyox powder in ethylene glycol, and then dissolving this mixture into a few liters of water. We used a slow magnetic stirrer over long periods of time to achieve a uniform concentration without mechanically degrading the polymer. This concentrated polymer solution was gently poured into the tank to which water was subsequently added to fill it up. The contents of the tank were mixed by gently pulling the grid up and down a few times. The polymer solutions were clear and translucent, and their optical properties stable over the course of the experiment.

The surfactant solution was prepared by mixing it in a few liters of water by gently stirring the solution. The tank was filled with water to which the appropriate amount of sodium salicylate was added. The surfactant solution was then added to the contents of the tank. As before, the grid was manually traversed up and down to achieve uniform

mixing. The surfactant solution was translucent but with a greenish tint. This coloring increased in intensity over the course of a day; towards the end of the day, the fluid absorbed too much of the red laser light for the PIV system to function properly. This is the principal reason for the smaller size of data collected for surfactants.

Following these steps, the seeding particles were added and the fluid was stirred slowly with the grid. Allowing the fluid to sit still for a few hours, after this last step, not only resulted in the larger seeding particles to settle to the tank bottom—as noted already—but also allowed the entrapped air bubbles to rise to the surface.

III. RESULTS

Figure 2(A) shows the decay with time of the mean square velocity for the longitudinal velocity component, $\langle u'^2 \rangle$, and transverse velocity component, $\langle v'^2 \rangle$. Here, $\langle \cdot \rangle$ represents ensemble averaging. The decay data for both components appear to follow two power laws, $(t/t_M)^{-\alpha}$. The exponent for time periods of up to about 1000 mesh times is about 1.1 for both components; for larger times, it is about 1.5. We have used no virtual origin.

In grid-turbulence studies in wind tunnels, the decay exponent for the first few hundred mesh distances has been measured to be about 1.2.¹⁴ The corresponding exponent seems to be somewhat smaller for towed grids.¹⁵ This difference is believed to be partly an effect of the degree of anisotropy at the start of the decay process. This is a topic for separate discussion; it surfaces to say here that the present data are consistent with the initial period of decay for classical grid turbulence.

At $t/t_M \approx 1000$, the nominal value of the integral length scale, estimated from the empirical formula given by Sreenivasan *et al.*,¹⁴ is expected to be about 3 cm. Turbulent fluctuations are correlated for significantly greater distances than the integral length scale, so it is reasonable to think that they begin to feel the walls of the tank sometime around this point. (Directly measured length scales, obtained from the PIV data, were consistent with this estimate; however, we have not shown the length-scale data here primarily because the correlations obtained from the fixed PIV domain are not accurate enough for large separation distances.) The analysis of turbulence decay, appropriate to the case of saturated length scale, can be found in Smith *et al.*¹⁶ In that paper, it is shown that the exponent should be larger, qualitatively consistent with the present measurements. A more detailed analysis of this aspect can be found in Skrbek and Stalp.¹⁷

The decay rates of the mean-square velocity fluctuations in longitudinal and transverse directions are roughly the same at all times considered here. The ratio of the energy components is about 1.25. This degree of anisotropy is characteristic of the grid data.^{18,19} Thus, the present grid turbulence in water can be said to behave as expected.

Figures 2(B) and 2(C) show the decay of the mean-square energy components for the polymer and surfactant solutions. There are some differences between water and the DRA solutions. First, the longitudinal and transverse components of energy have different decay rates in both polymer

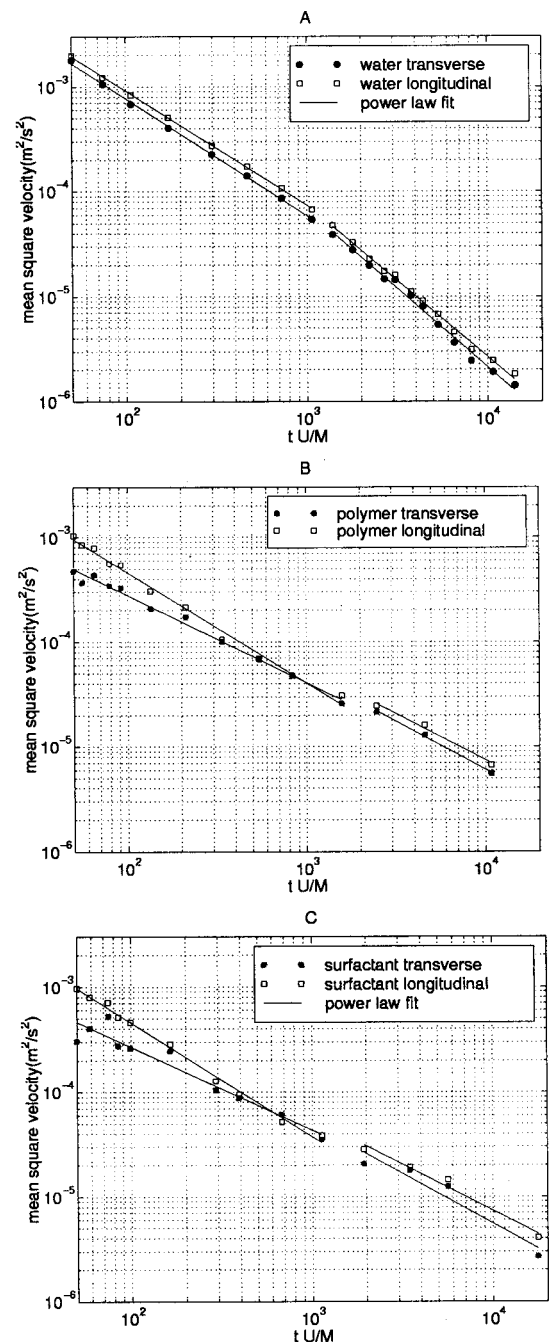


FIG. 2. Mean square velocity fluctuations in the longitudinal and transverse directions ($\langle u'^2 \rangle$ and $\langle v'^2 \rangle$, respectively) vs t/t_M for (A) water, (B) polymer (100 ppm), and (C) surfactant solution (5.0 mM, with 12.0 mM sodium-salicylate). Linear least-squares fits in the two scaling regions are shown. The decay exponents α are noted in Table II. The uncertainty in the exponents is given by the standard error of the fit.

and surfactant solutions. In each case, the longitudinal component initially has about the same decay exponent as for water, while the transverse energy component decays more slowly. Beyond the point at which the new power-law sets in (about $1000t_M$), the two components in each case decay more or less at the same rate, this being substantially slower than that in water. Table II lists the decay exponents in the two power-law regions for all three cases. That there is initial anisotropy for polymers and surfactants is reconfirmed from

TABLE II. Decay exponents for initial and later periods for water, polymer, and surfactant solutions. The fits for the initial and later periods of decay are separated by $t_M=1000$.

Fluid (concentration)	Initial period		Later period	
	α (longitudinal)	α (transverse)	α (longitudinal)	α (transverse)
polymer (100 ppm)	1.06 ± 0.08	0.84 ± 0.08	0.89 ± 0.19	0.92 ± 0.10
surfactant (5.0 mM/12.0 mM)	1.09 ± 0.08	0.79 ± 0.19	0.88 ± 0.19	0.96 ± 0.38
water	1.09 ± 0.03	1.12 ± 0.02	1.45 ± 0.07	1.50 ± 0.10

Fig. 3 which shows the energy ratios as a function of time. Unlike water turbulence for which isotropy holds roughly for all times measured (longitudinal/transverse energy ratio ≈ 1.25), the polymer and surfactant solutions are strongly anisotropic initially.

As shown in Fig. 3, the most conspicuous disparities between water and DRAs occur at the early stage of decay. Taking polymer solutions first, and considering $50t_M$ as typical, we find that the Zimm relaxation time for the polymer is several times smaller than the maximum inverse strain-rate in turbulence. It does not therefore seem likely that the polymers are stretched to any degree once the homogeneous state of turbulence is established. The bulk of the stretching must therefore occur before the merger of the wakes from individual grid-rods occurs, perhaps in boundary layers around the rods. A similar qualitative argument can be made for surfactants as well.

In spite of this difference, we have already noted that the energy decay rate for the two DRAs is similar. This is qualitatively analogous to pipe flows, where the effects of both DRAs are similar on drag reduction. To see the differences further, we focus our attention on the spatial structure at the fixed mesh time of $50M/U$. Although a fixed value of mesh times does not correspond to an identical eddy-turnover time in all cases, it does enable us to make comparisons when the effects of the DRAs are most pronounced. That some of the differences can be spectacular is seen in Fig. 4, which plots typical instantaneous velocity vectors in the region A of Fig. 1. The images there extend over 1.6×1 meshes for $t_M=50$,

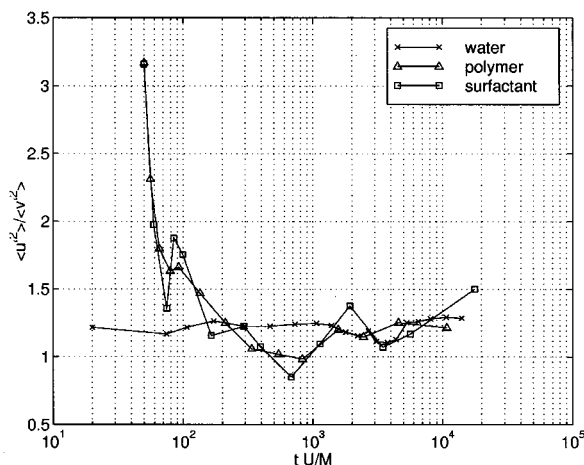


FIG. 3. The ratio of the longitudinal to transverse energy components. The polymer and surfactant concentrations are the same as for Figs. 2.

and so capture a significant portion of the turbulent energy-containing scales. It is evident that small scales continue to exist in the surfactant case—perhaps even strengthened—but are far less apparent in the polymer case. The energy spectral densities in the two cases must therefore differ. We point out

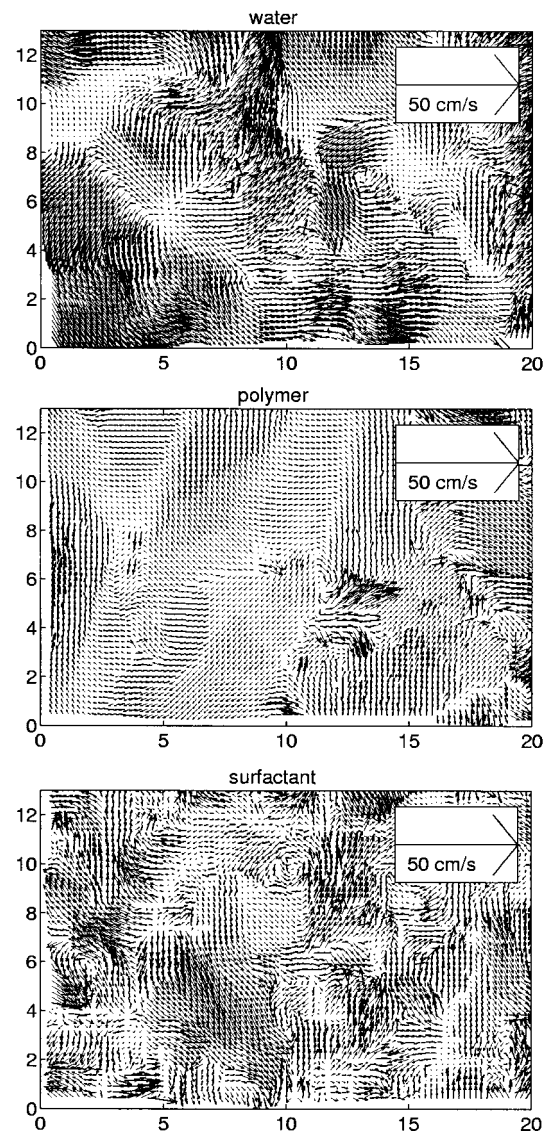


FIG. 4. Examples of PIV images in the area A for $t/t_M=50$. Top, water; center, polymer; bottom, surfactant. The dimensions of the images are in mm. Each arrow denotes the velocity (in the plane of the camera) averaged over a volume of dimensions $0.91 \text{ mm} \times 0.91 \text{ mm} \times 0.1 \text{ mm}$. The differences between polymer and surfactant images are not equally striking for all realizations, but the behavior displayed is representative. See text for more details.

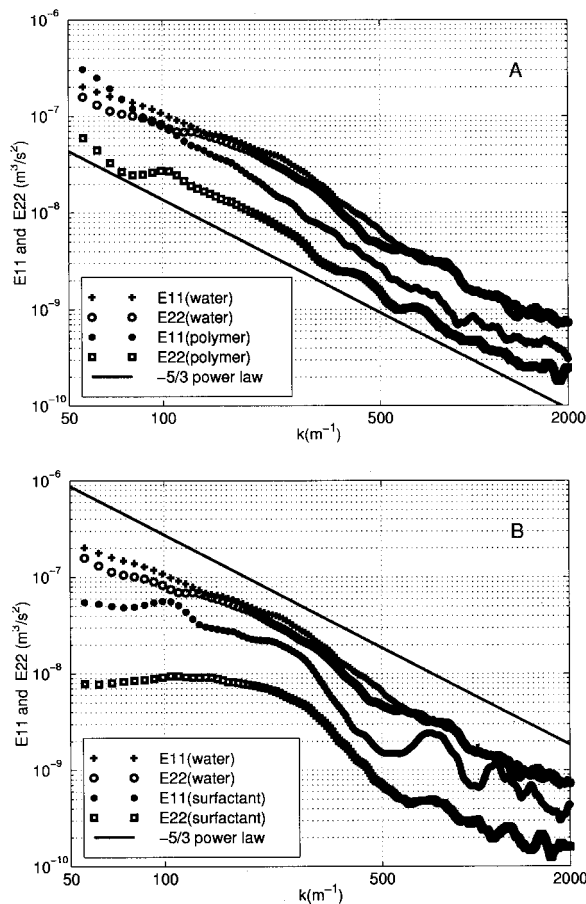


FIG. 5. Power spectra for the longitudinal (E_{11}) and transverse (E_{22}) velocity components at $t/t_M = 50$ for polymer (top) and surfactant (bottom) solutions. The additive concentrations are the same as for Figs. 2. Plotted for comparison are the spectra for water at the same time of development.

that PIV enables the measurement of wave number spectra without any recourse to Taylor's hypothesis. In Figs. 5(A) and 5(B) the spectral densities of polymer and surfactant data are compared with those of water, for $t/t_M = 50$. For comparison, we also plot a $-5/3$ power law. For both water and the polymer case, there is an approximate power-law region for wave numbers between 50 m^{-1} and 500 m^{-1} . The high wave number cutoff, determined by the size of the interrogation volume of the PIV analysis, corresponds to $k \approx 1000 \text{ m}^{-1}$. The size of the imaged area gives the low wave number cutoff at $k \approx 50$. There is no conspicuous power-law region for surfactants. In the low wave number range, the spectra for both DRAs exhibit a conspicuous bump at $k \approx 100 \text{ m}^{-1}$, corresponding to the grid mesh. A similar bump is not apparent in the water spectra. Presumably, the viscoelastic nature of the DRAs exhibit a long memory effect of the initial forcing. The longitudinal data for surfactants exhibit another large bump at $k \approx 800 \text{ m}^{-1}$, for which we have no satisfactory explanation.

The attenuation of the high-frequency energy for the polymer is clear in the PIV image of Fig. 4. The depletion of energy (compared to water) occurs in both energy components, though the large-scale in the longitudinal component does not differ by much. These results are consistent with

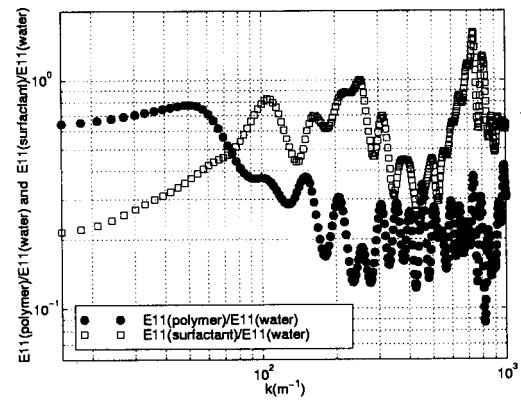


FIG. 6. Ratio of the spectral densities (E_{11}) of polymer and water, and of surfactant and water. The additive concentrations are the same as for Figs. 2.

those of McComb *et al.*⁹ in grid turbulence and of Tong *et al.*²⁰ in the Couette geometry, with one possible exception. This exception corresponds to the observation of a threshold concentration by McComb *et al.*,⁹ similar to the well-documented effect in pipe flows.³ We did not observe this threshold effect even though our lowest concentration was below McComb's threshold. A possible explanation is that our polymer had a molecular weight which is about twice that used by McComb *et al.* For pipe flow, it is known that the threshold concentration decreases with increasing molecular weight³ according to a relatively large power of the molecular weight (or the number of coils in the monomer). We should therefore expect the threshold concentration, if one exists, to be much lower in our experiments.

In the surfactant case, even the large-scale energy is substantially diminished. This effect cannot be explained by the increased viscosity of the surfactant solution as compared to water (because the large scale motion in turbulent flows is expected to be independent of the Reynolds number). The scale-dependent depletion effects in polymers and surfactants can be seen better in Fig. 6 which plots against the wave number the longitudinal spectral density as a fraction of that of water. The ratio for the polymer decreases up to a wave number of about 200 m^{-1} , staying essentially constant thereafter. The ratio for the surfactant starts very low and increases up to a wave number of about 240 m^{-1} and then drops off up to a wave number of about 600 m^{-1} . We again observe a large unexplained increase at a wave number of $k \approx 800 \text{ m}^{-1}$. The ratio for the transverse component is identical for the surfactant, but essentially constant over all wave numbers for the polymer.

Thus, the polymers and surfactants possess significant structural differences as well as statistical similarities. We shall now discuss some more similarities. The scatter plots of u vs v (Fig. 7) show that, in contrast with water, excessive fluctuations are removed in both DRA cases. The direction of velocity vector in the plane of circulation provides another measure of the organization of the fluctuations; relatively little attention has been paid in the past to direction statistics. We present in Fig. 8 the probability density functions of the direction θ of the velocity vectors ($\theta = \tan^{-1}(v/u)$) in the (x, y) plane. For water, there is a small anisotropy between

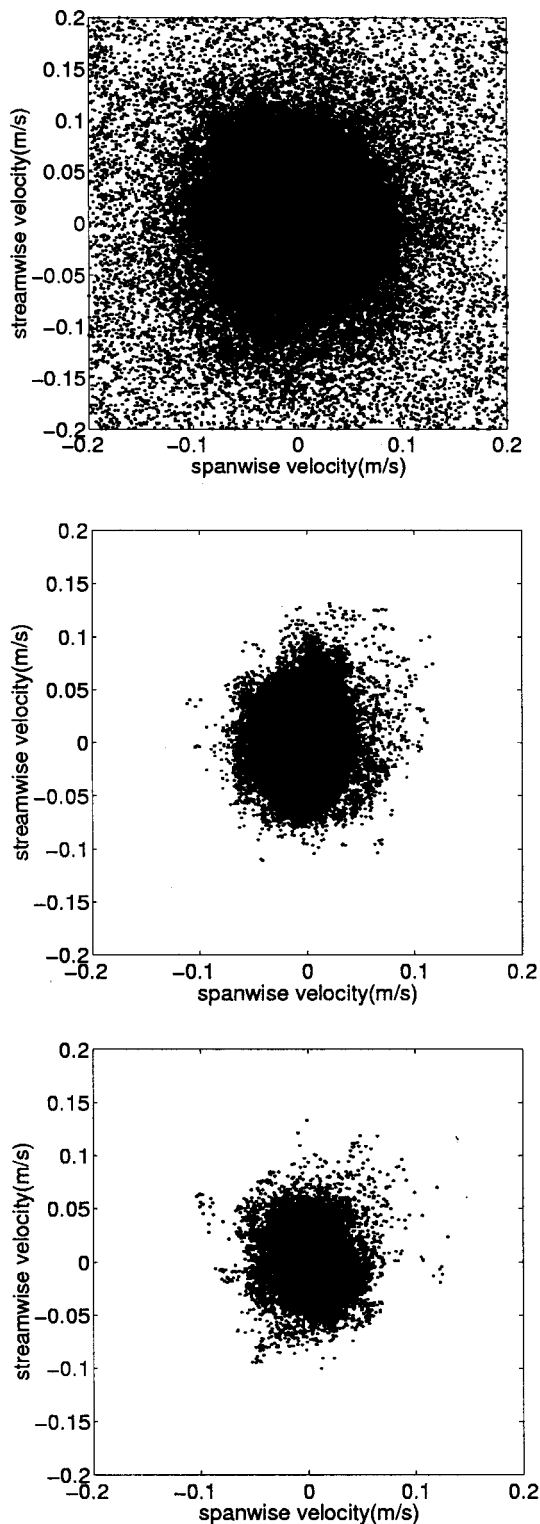


FIG. 7. Scatter plots of longitudinal and transverse velocity fluctuations at $50t_M$. Top, water; center, polymer; bottom, surfactant.

the longitudinal direction, possibly due to a small vertical mean flow in the measurements. However, for the polymer and the surfactant, the longitudinal direction is more prevalent than the transverse. In this sense, the anisotropy observed in polymer and surfactant solutions is similar to that in the wall-region of the boundary layers in Newtonian

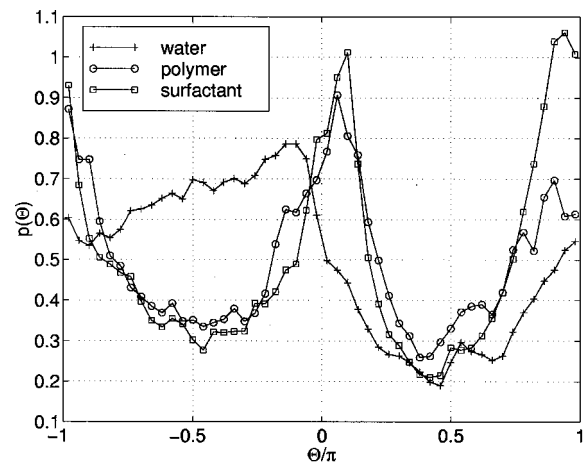


FIG. 8. Probability density functions of the directions of the velocity vectors. Here $\theta=0$ corresponds to up, $\theta=\pi$ to down, $\theta=-\pi/2$ to left, and $\theta=\pi/2$ to right.

flows.²¹ It is also observed that the values for the surfactant at $\theta=\pm\pi$ and 0 are significantly greater than those for the polymer.

The results discussed in this section are for the highest concentration polymer and surfactant solutions. They are qualitatively the same for lower concentrations, and are quantitatively somewhere between those for water and those for the high concentration solutions. As already mentioned, we did not observe any “threshold concentration” effects in the range of parameters studied.

IV. SUMMARY AND CONCLUSIONS

A basic reason for undertaking the present experiments was to understand better whether DRAs can have a strong effect in homogeneous turbulence outside the near-wall region of a pipe flow. From a first glance, the present measurements indeed show that the nearly homogeneous turbulence behind towed grids is significantly affected by polymer and surfactant addition. The chief difference between water on the one hand and the DRA solutions on the other is that the turbulence structure in the latter becomes more anisotropic, and large-amplitude, small-scale, fluctuations are damped selectively. A closer look reveals that the situation is probably more complex. The bulk of the stretching of the polymers occurs in boundary layers around the rods, or, perhaps in their individual wakes. The initial development is thus the most crucial part of the process. In this region, we observe large anisotropy for polymer and surfactant solutions. A plausible explanation for polymer solutions is that the polymers are stretched and oriented vertically as the grid is pulled through the solution. In the subsequent decay, the stretched polymers dampen the transverse fluctuations strongly. This important conclusion would have been lost in one-dimensional measurements. The strong anisotropy of the polymer solutions could also explain the findings of two distinct threshold concentrations from spectra and visualization experiments.⁹

The effects of polymers and surfactants are similar in some respects and different in some others. The main point of similarity is the reduced rate of decay. The major difference is that the small scales are more selectively damped in polymers than in surfactants. This can mean that the net reduction in the energy decay rate, which is about the same in both cases, has been attained through different paths in the two cases. This conclusion supports the view that the mechanism for drag reduction could be different between polymers and surfactants.

The differences between surfactant and polymer solutions may perhaps be understood in terms of their disparate viscoelastic natures. Polymer solutions impart viscoelasticity due to stretching of individual molecules under high extensional strain of the small scale. The suppression of small scales may ensue from an elastic absorption of energy on those scales, resulting in a truncation of the cascade (or cascadelike activity), as suggested by de Gennes.⁴ When the polymer molecules move to regions of lower shear, they may return the stored elastic energy to the flow resulting in a decrease in the decay rate of turbulence. For surfactant solutions, the formation of network structures may interact directly with the large scale structure of turbulence, absorb and return elastic energy in much the same manner as suggested for polymer molecules.

The present measurements allow us to make a general observation on drag reduction in boundary layers and pipes. The response to polymer addition in any inhomogeneous flow depends strongly on where in the flow—and perhaps also on how—the injection occurs. Even if the elastic theory were correct, the major effect is likely to occur near the wall rather than in the bulk of the flow. A more detailed discussion of this aspect can be found in Sreenivasan and White.²²

ACKNOWLEDGMENTS

It is a pleasure to dedicate this article to Robert H. Kraichnan on the occasion of his 70th birthday. We thank the referees for their helpful remarks. This research was supported by the NSF Grant No. DMR-9529609.

¹R. H. Nadolink and W. W. Haigh, "Bibliography on skin friction reduction with polymers and other boundary-layer additives," *ASME Appl. Mech. Rev.* **48**, 351 (1995). This is a complete bibliography of the effects of additives until the early 1990s.

²J. L. Lumley, "Drag reduction by additives," *Annu. Rev. Fluid Mech.* **1**, 376 (1969).

³P. S. Virk, "Drag Reduction Fundamentals," *AIChE. J.* **21**, 625 (1975).

⁴P. G. de Gennes, *Introduction to Polymer Dynamics* (Cambridge University Press, Cambridge, 1990).

⁵J. M. J. Den-Toonder, M. A. Hulsen, G. D. C. Kuiken, and F. T. M. Nieuwstadt, "Drag reduction by polymer additives in a turbulent pipe flow: numerical and laboratory experiments," *J. Fluid Mech.* **337**, 193 (1997).

⁶For a recent effort, see, O. Cadot, D. Bonn, and S. Douady, "Turbulent drag reduction in a closed flow system: Boundary layer vs bulk effects," *Phys. Fluids* **10**, 426 (1998).

⁷For a summary of various perspectives on this problem, see *Self-Sustaining Mechanisms of Wall Turbulence*, edited by R. Panton (Computational Mechanics, Southampton, 1997).

⁸C. A. Friehe and W. H. Schwartz, "Grid-generated turbulence in dilute polymer solutions," *J. Fluid Mech.* **44**, 173 (1970).

⁹W. D. Mcomb, J. Allan, and A. Greated, "Effect of polymer additives on the small-scale structure of grid generated turbulence," *Phys. Fluids* **20**, 6873 (1977).

¹⁰J. L. Zakin, J. Myska, and Z. Chara, "New limiting drag reduction and velocity profile asymptotes for nonpolymeric additives systems," *AIChE. J.* **42**, 3544 (1996).

¹¹I. L. Povkh, A. V. Stupin, and P. V. Aslanov, "Structure of turbulence in flows with surfactant and polymeric additives," *Fluid Mech.-Sov. Res.* **17**, 165 (1998).

¹²K. R. Sreenivasan, "On the scaling of the turbulence energy dissipation rate," *Phys. Fluids* **27**, 1048 (1984).

¹³M. Raffel, C. Willert, and J. Kompenhans, *Particle Image Velocimetry: A Practical Guide* (Springer, Berlin, 1998).

¹⁴For a collection of data in this respect, see, K. R. Sreenivasan, S. Tavoularis, R. Henry, and S. Corrsin, "Temperature fluctuations and scales in grid-generated turbulence," *J. Fluid Mech.* **100**, 597 (1980).

¹⁵M. D. Walker, "Laser Doppler measurements of grid turbulence in a box," Ph.D. thesis, Johns Hopkins University, Baltimore, 1986.

¹⁶M. R. Smith, R. J. Donnelly, N. Goldenfeld, and J. Vinen, "Decay of vorticity in homogeneous turbulence," *Phys. Rev. Lett.* **71**, 2583 (1993).

¹⁷L. Skrbek and S. R. Stalp, "On the decay of homogeneous isotropic turbulence" (preprint, 1999).

¹⁸H. Sato, "Experimental study of the spectrum of isotropic turbulence. I," *J. Phys. Soc. Jpn.* **6**, 387 (1951).

¹⁹G. Comte-Bellot and S. Corrsin, "Simple Eulerian time correlation of full and narrow-band velocity signals in grid-generated, isotropic turbulence," *J. Fluid Mech.* **48**, 271 (1970).

²⁰P. Tong, W. I. Goldburg, and J. S. Huang, "Measured effects of polymer additives on the turbulent-velocity fluctuations at various length scales," *Phys. Rev. E* **45**, 7231 (1992).

²¹P. Kailasnath, "Reynolds number effects and the momentum flux in turbulent boundary layers," Ph.D. thesis, Yale University, 1993.

²²K. R. Sreenivasan and C. M. White, "The onset of drag reduction by dilute polymer additives, and the maximum drag reduction asymptote" (preprint, 1999).